Proceedings of the
44th IEEE Conference on Decision and Control, and
the European Control Conference 2005
Seville, Spain, December 12-15, 2005

Maglev Apparatus for Power Minimization and Control of Artificial Hearts

Chandrasekhar Samiappan, Nasim Mirnateghi, Brad E. Paden, *Fellow, IEEE,* James F. Antaki, *Member*, *IEEE*

Abstract— **This project is directed at the third generation of heart pumps being developed in commercial research laboratories which employ feedback-controlled magnetically levitated pump impellers. Unique features of the control problem are the quasi-periodic pressure disturbances of the natural heart and nonlinearities of the magnetic levitation system. The main motivation for this paper is the power consumption due to quasi-periodic pressure disturbances from the natural heart. Since clinical studies are not possible for the vast majority of our work, there is a need for an apparatus to simulate the Left Ventricular Assist Device (LVAD) for controller design. Inspired by this need, we design a novel experimental apparatus to study the Maglev LVADs. We develop a nonlinear model, then a linearized model followed by simulation and stabilization of the closed loop system using a Virtual Zero Power (VZP) controller.**

I. INTRODUCTION

CONGESTIVE heart failure remains a leading cause of morbidity and mortality around the world and heart transplantation, the only accepted method to treat severe cases of the disease, cannot meet the vast demand. Left ventricular assist devices (LVADs) are an emerging treatment for the thousands of patients suffering from end-stage heart disease. These "artificial hearts" are implanted and cooperate with the natural heart in pumping blood. The current (second generation) pumps are rotary pumps that use the blood itself as a lubricant in fluid film bearings. This project is directed at the third generation of pumps being developed in commercial research laboratories which employ feedback-controlled magnetically levitated pump impellers (e.g. MedQuest's HeartQuest LVAD).

Magnetic levitation eliminates mechanical wear and shear-induced damage to the blood (red blood cells, platelets and leucocytes). Motivated by these benefits of magnetic levitation, the first magnetically levitated pump was implanted in an animal trial at the University of Pittsburgh in 1998[1, 6]. The technology was enabled by feedback control, advances in magnetic materials and systematic optimization of the controlled plant. However, the small size, short time constants, nonlinearity, instability and quasi-periodic disturbances from the natural heart pose an awesome challenge to control engineers. In this paper, we design a complete experimental apparatus to study the levitation system in these artificial hearts for power consumption and control. The experimental Maglev plant has one active degree of freedom – the axial direction with complete magnetic levitation. It is compact and presents an excellent laboratory base for doing maglev and artificial heart experiments. A unique aspect of the design is the use of linear voice coil actuators for axial displacements and not purely passive radial levitation. The apparatus has fast time constants similar to Maglev LVADs in commercial development.

The Maglev plant is used in the experimental apparatus (Fig.2 & 4). We develop a nonlinear model of the plant by combining models for each of the plant components which are nonlinear (bearing force nonlinearity, nonlinear actuator force sensitivity and sensor nonlinearity – See Table I). Stabilization of the system is achieved using a Virtual zero power (VZP) controller consisting of a PD position control with integral feedback which nulls out the control signal (as opposed to position error). The VZP controller not only stabilizes the plant but also minimizes power consumption of the control actuator in the presence of DC disturbances. Finally, closed loop identification is used to estimate the parameters and validate the model.

Manuscript received March 5, 2005. This work was supported in part by the National Science Foundation under Grant NSF/ECS-0401267. The work of Prof. J.F.Antaki was supported in part with Federal funds from the National Heart, Lung, and Blood Institute, National Institutes of Health, under Contract No. HHSN268200448192C.

C. Samiappan is with the University of California, Santa Barbara, CA 93106 USA (e-mail: sekhar@engr.ucsb.edu).

N. Mirnateghi is with the University of California, Santa Barbara, CA 93106 USA (e-mail: nasim@ece.ucsb.edu).

Corresponding author, B.E. Paden is a fellow of IEEE and is with the University of California, Santa Barbara, CA 93106 USA (phone: 805-895-8165; fax: 805-893-8651; e-mail: paden@engr.ucsb.edu).

J.F.Antaki is with the Carnegie Mellon University, Pittsburgh, PA 15213 USA (e-mail: antaki@andrew.cmu.edu).

0-7803-9568-9/05/$20.00 ©2005 IEEE

II. Connection to the Artificial Heart

Maglev artificial hearts have a magnetically levitated rotating impeller, which is supported on permanent magnet radial bearings. This design radically improves reliability, improves the quality of the blood flow through the pump and nearly eliminates blood damage. For these reasons magnetic levitation and the associated control system are essential ingredients of the next generation of artificial hearts. The rotor is magnetically controlled in six degrees of freedom but only two degrees of freedom are actively controlled – the axial and rotational motions. By Earnshaw's theorem [4], the sum of the linear stiffnesses is zero, so there is at least one axis along which the position is unstable. The symmetry about the axial axis renders the rotational stiffness zero and the axial stiffness is negative creating the axial instability. The pulsation of the native heart creates a quasi-periodic load (axial disturbance) on the LVAD levitation system that increases power consumption of the levitation actuator dramatically. The objective is to design controllers to reject these axial disturbances and minimize the power consumption. The experimental apparatus can help in accomplishing this goal.

MedQuest Inc.'s Heartquest based on the Streamliner artificial heart [1] and University of Pittsburgh's Pediaflow are the some of the third generation LVADs in various advanced stages of development. The concept of Pediaflow system is shown in Fig.1. Pediaflow is a magnetically levitated pump for infants having a suspension similar to the Streamliner. The maglev pump draws blood from the apex of the left ventricle and pumps blood, in parallel with the left ventricle, into the aorta of the infant.

Fig 1. University of Pittsburgh's, PediaFlow™ system.

From a control's perspective, we can treat the magnetically levitated rotor in the artificial heart as a magnetically levitated mass. Also, since we need to study only axial disturbances, we design a novel setup with one active degree of freedom plant. We design the magnetic stiffness and the levitated mass in our plant to match the time constants of the artificial hearts. The control actuator in the plant provides levitation and control for the plant. Our plant has a disturbance actuator which can be used to simulate the pulsations caused by the heart in an experimental setting. The designed controllers can be easily implemented on the plant using the apparatus shown in Fig.2.

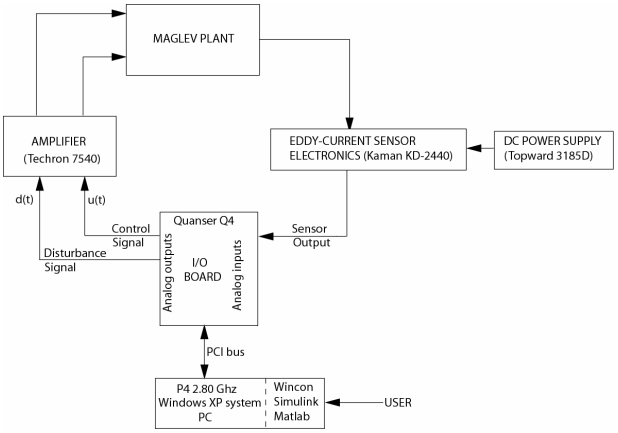

Fig.2. Sketch of the entire experimental apparatus (Refer Table I for component detail)

III. Experimental Apparatus

TABLE II
SYSTEM PARAMETERS

Component (# used)	Description
Maglev plant (1)	Refer to Maglev plant design
I/O board (1)	Q4 H.I.L. board, Quanser Consulting Inc, Ontario, Canada. *Key Specs*: 4 A/D channels, 4 D/A channels, Integrated to Matlab/Simulink via Quanser Wincon.
Eddy current sensor (1) with the electronics module (1)	KD-2440 with 5 CM sensor, Kaman Aerospace Corporation, Middletown, CT. *Key Specs*: Standard Range: 2.54 mm for Aluminum target, Freq. Response: 0 – 10 Khz. Sensor equation: $y(V)=-4.7055x^2\ (mm)+4.7693x(mm)$
Linear Voice-coil actuators (2)	LA 13-12-000A, BEI Technologies Inc, San Marcos, CA. *Key Specs*: Continuous Stall force: 7.12 N, Motion range: 6.35 mm, DC resistance: 17.1 ohms, Max force sensitivity: 9.79 N/amp. Force sensitivity equation: $K_f\ (N/amp)=-0.1735x^2\ (mm)+0.0777x(mm)+9.79$
Amplifier (1)	Techron 7540, AE Techron Inc, Elkhart, IN. *Key specs:* Dual channel, freq response: 0 to 100 kHz, Variable gain set to 10 V/V.
DC power supply (1)	3185D, Topward electric instruments co. Ltd, Taiwan. *Key specs:* 0 – 18 V, 5 amp, digital metering.
PC(1)	Dell Workstation PWS 360, Dell Inc. *Key Specs:* P4 2.80 GHz Windows XP system.
Digital Oscilloscope(1)	TDS 3014B, Tektronic, Beaverton, OR. *Key specs:* 4 channel digital oscilloscope.

The maglev plant has been the primary focus of this work since it simulates the levitation dynamics in its actual setting. Other components of the apparatus as indicated in Fig. 2 and Table I, include an I/O board which serves as the data acquisition board interfacing the PC and the maglev plant, an eddy current sensor for sensing the axial displacements in the system, a pair of linear voice-coil actuators for providing control and disturbance signals from the PC to the system in the form of axial actuations, an amplifier to drive the actuators, a DC power supply to power the sensor and a digital oscilloscope to observe the signals in the circuit. The voice coil actuators are connected to the computer through the DC amplifier operating in the voltage mode, the terminal board and the data acquisition card in that order. The eddy current sensor is interfaced to the computer through the sensor electronics module (which is powered by DC power supply), the terminal board and the data acquisition again in that order.

A. Maglev Plant Design

A cross section of the Maglev plant, shown in Fig. 3, depicts the compact design that combines the linear voice-coil actuators, radial PM bearings and the levitating shaft. The main levitating part of the system is the shaft supported by a pair of permanent magnet (PM) radial bearings on either side.

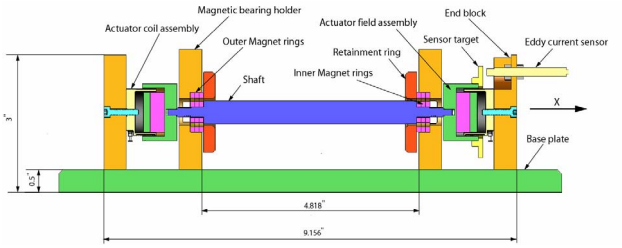

Fig.3. Section view of the Maglev plant showing major dimensions (inches) and main component details. X refers to the axial displacement of the shaft

The essential design parameters are the axial stiffness of the magnetic bearing (-25.45 [N/mm]) and the levitating mass (0.3573 [Kg]) which, together, determine the unstable mechanical time constant of the system. The artificial heart time constants dictate the time constants of the system.

As a consequence of Earnshaw's theorem [4], it is not possible to stably levitate a body solely with permanent magnets at an equilibrium point of the static magnetic field. In our case there are two radially directed eigenvectors and one axially directed eigenvector of the stiffness matrix. Indeed, the axial stiffness has opposite sign and twice the magnitude of radial stiffness for each radial bearing [3]. This negative axial stiffness gives axial instability and hence, axial positioning of the levitating mass poses an interesting control problem. When rings of the inner and outer stacks are aligned, the shaft is in an axial equilibrium – this is defined as the $x = 0$ point. The pull-in range of the shaft is determined by the axial magnetic stiffness and the peak force of the control actuator.

TABLE II
SYSTEM PARAMETERS

Parameter symbol	Parameter description	Parameter value
m	Levitated mass	0.3573 Kg
k	Axial stiffness (both bearings)	25,450 N/m (designed) 30,200 N/m (actual)
λ	Spatial wavelength of the magnet array in the bearing	5 mm
Ga	D.C Amplifier current gain	0.586 amp/V
Kf	Actuator force sensitivity	9.79 N/amp
go	Gap between the inner & outer magnet arrays when centered	2 mm
L	Axial length of each bearing	7.5 mm
R	Average radius of the bearing	7 mm
Br	Remanence of the magnetic material used in the bearing	1.2 Tesla (NdFeB, N42)
d	Thickness of the magnet rings	3 mm
μ_0	Permeability of vacuum	$4\pi\times10^{-7}$ $WbA^{-1}m^{-1}$
N	No. of magnet rings in each bearing	3
La	Actuator coil inductance	2.8 mH
Ra	Actuator coil resistance	17.1 ohms
g	Acceleration due to gravity	9.8 m/s^2
-	Controller Sampling rate	10 KHz
-	Pull-in range (mechanical)	0.8 mm

The main elements of the plant are the Permanent Magnet bearing, the linear voice-coil actuators and the sensor. Therefore, we first model the main elements to develop a model for the entire plant.

B. Permanent Magnetic Bearing Modeling and Design

The axial cross-section of a general magnetic bearing is shown in Fig. 4. The magnet bearing is formed from concentric magnet rings of rectangular cross-section. An

outer stack of three magnet rings is mounted on the magnetic bearing holder while the inner stack of three magnet rings is mounted on the shaft. The number of rings in each bearing is an important parameter which affects the magnetic stiffness of the setup. When the inner and the outer magnet rings are exactly aligned one over the other, we get zero axial magnetic force. The stiffness levels in PM bearings can be considerably improved by stacking together thin PM magnets and narrowing the gap between inner and outer stacks [2]. Interestingly, an axially magnetized bearing has same load capacity and stiffness as the radially magnetized bearing [3]. Hence, the easier-to-manufacture axially magnetized magnets are used here.

Neodymium-Iron-Boron was chosen as the material of the magnet rings because it has the highest energy product for size and is cost effective.

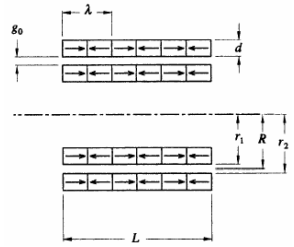

Fig.4. Axial cross-section of the permanent magnet (PM) bearing

The expression for radial stiffness of a radial PM bearing (for a unit cross-sectional area) is given by [2]

$$k_r = \frac{4Br^2}{\lambda\mu_0} \sum_{n=1(odd)}^{\infty} \{\frac{(1-e^{-n2\pi d/\lambda})e^{-n2\pi g_0/\lambda}}{n}\} \quad (1)$$

The above expression is valid for the assumption of negligible end-effects (i.e. $L >> \lambda$) which is not quite true for our setup. A correction factor of (2n-1)/2n is applied based on a count of interacting magnets, with (1) to adjust for end effects. Recall that the axial stiffness of the bearing is twice the radial stiffness of the bearing. Using these adjustments, we get the following expression for the destabilizing axial stiffness of the bearing:

$$k = \frac{(32LR)(2n-1)(Br^2)}{2n\lambda\mu_0} \sum_{n=1(odd)}^{\infty} \{\frac{(1-e^{-n2\pi d/\lambda})e^{-n2\pi g_0/\lambda}}{n}\} \quad (2)$$

While designing for magnetic stiffness, it is important to ensure that the radial displacement of the shaft due to gravity does not cause contact between the inner and outer races. Mathematically,

$$g_0 >> \frac{mg}{2k_r} \quad (3)$$

An opposing constraint for high magnetic stiffness comes from the maximum sampling rate that the data acquisition boards available in the market can achieve. The sampling rate should be roughly 6-10 times the bandwidth to avoid excessive controller phase lag. Variations in PM material properties lead to actual stiffness differing from the designed stiffness by up to 20%. This could also be due to machining tolerances, improper alignment of the bearing or variation in the surrounding temperature. The designed stiffness of our system was k = 25,450[Nm^{-1}] but the actual stiffness computed using system identification (refer section V) was k = 30,200[Nm^{-1}] which shows a variation of about 18% which is typical by our experience.

IV. MODELING

The radial magnetic bearing is comprised of a periodic array of permanent magnets and for moderate axial displacements, has a nonlinear spring force of the form

$$Fspring = k_n \sin(x/\lambda) \quad (4)$$

where x is the axial displacement of the system. The factor k_n is positive so that the uncontrolled axial motion is unstable. The axial control force applied to the shaft is accomplished with a voice-coil actuator whose force constant varies from a peak, when the magnet is centered in the coil, and decreases as the coil is moved along the axis of the actuator. Thus the control actuator force as a function of the control voltage, *u*, is modeled as

$$F_{control} = K_f(x)G_a u \quad (5)$$

The disturbance actuator force as a function of the disturbance voltage, d, is modeled as

$$F_{disturbance} = K_f(-x)G_a d \quad (6)$$

The reason for the negative sign in the disturbance actuator force is the opposite orientation of the actuators.

Now, *m* is the levitated mass of the system so the force balance equation leads to the combined axial dynamics:

$$m\ddot{x} = F_{spring} + F_{control} + F_{disturbance} \quad (7)$$

A. Nonlinear Model

The non-linear model of the system is given by

$$m\ddot{x} = k_n \sin(x/\lambda) + K_f(x)G_a u + K_f(-x)G_a d \quad (8)$$

The bearing force is the pre-dominant nonlinearity in the system. But, since the maximum displacement in the system is constrained to $\pm 0.4mm$, the bearing force non-linearity is within 0.1 %. Approximating the nonlinearity by linear terms,

$$k_n \sin(x/\lambda) \approx k_n x/\lambda = kx \quad (9)$$

$$K_f(x) \approx K_f \quad (10)$$

$$F_{control} = (G_a K_f)u, F_{disturbance} = (G_a K_f)d,$$

$$F_{spring} = kx \quad (11)$$

B. Linearized Model

Substituting (9) & (10) in the non-linear equation (8),

$$m\ddot{x} = kx + (G_a K_f)u + (G_a K_f)d \quad (12)$$

The system is modeled as a second-order ordinary differential equation after linearizing the equation
The state space equations are given by

$$\dot{x}_1 = x_2$$

$$\dot{x}_2 = (k/m)x_1 + (G_a K_f/m)u + (G_a K_f/m)d \quad (13)$$

$$y = x_1$$

Here x_2 denotes the velocity of the system and the model parameters are listed in table I.
For the state space vector $x = [x_1\ x_2]^T$ with no disturbance,

$$\dot{x} = Ax + Bu$$
$$y = Cx \quad (14)$$

where the state space matrices *A, B* and *C* are defined as :

$$A = \begin{pmatrix} 0 & 1 \\ k/m & 0 \end{pmatrix}, B = \begin{pmatrix} 0 \\ G_a K_f/m \end{pmatrix}, C = [1\ 0], D = 0 \quad (15)$$

and the plant transfer function is

$$G = \frac{G_a K_f}{(ms^2 - k)} \quad (16)$$

The uncontrolled system has its only equilibrium point at the zero point. Now, since the system has unstable magnetic stiffness in the axial direction, the zero point is an unstable equilibrium point. The poles of the system are located at $\pm\sqrt{k/m}$ reflecting the instability in the axial direction. The system poles using actual stiffness are calculated to be at ± 290.7 rad/s and the time constant is 21.61 milliseconds. The natural frequency of the system is 46.3 Hz which gives the system fast unstable dynamics.

V. Stabilization and ID

A. Stabilization

The linearized system with the VZP controller is shown in Fig.5. The low-pass filter, the inverted nonlinear sensor mapping and the VZP controller were implemented in Simulink. Stabilization of the system is required to perform system identification. Stabilization can be achieved using a negative feedback through VZP controller. [5] Although simple, this control has the interesting property of exploiting the instability in the mass/negative spring system to cancel DC disturbances with zero power. With a DC disturbance applied, the rotor is displaced so that the spring force (not the control force) balances the DC disturbance. This is an important example of how plant instability can be used to reduce the control effort. In control terminology, it can be said that the VZP controller rejects the effects of static disturbances on the control input and minimizes power consumption of the system.

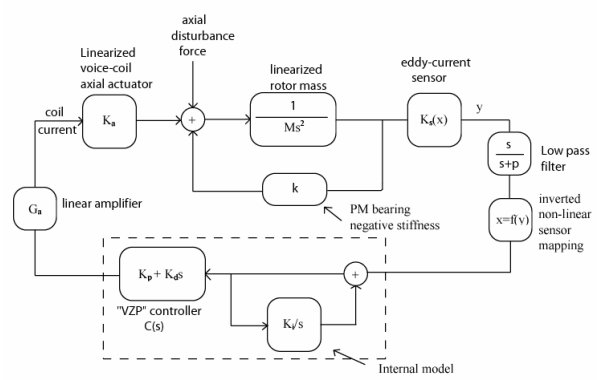

Fig.5. Linearized system with VZP controller for axial control.

In the absence of disturbance, the control cancels the negative spring force in steady state. Therefore, the axial displacement of the shaft is proportional to control input. Also, the VZP controller zeros the control input so that in the steady state in the absence of disturbance is $x = 0$ (the equilibrium of the PM bearings). The estimated displacement of the levitating mass is the feedback signal to the controller after filtering out the high frequency noise. The controller gain parameters are tuned experimentally to stabilize the system for closed-loop identification. Among the values of gain values that result in a stable closed loop are $K_i = 20$ (integrator gain), $K_p = 15000$ (proportional gain) and $K_d = 100$ (differentiator gain)

B. System Identification

Since the plant is unstable, the identification has to be carried out in closed loop. We used the joint input-output method of identification for estimating the parameters and validating the model because neither the noise model nor the controller model was required and we had easy access to all the signals in the closed loop.

In our case, the sensitivity and the closed loop transfer function were of order three which meant that the estimated plant had order six. Also, the higher order model had three stable and three unstable poles so the standard model reduction techniques couldn't be directly

applied. Therefore, we used a method in which we separated the stable and unstable subsystems and performed model reduction on each subsystem separately. At the end we pieced together both reduced order stable and unstable subsystems.

We obtained the overall reduced order model $\hat{G}$ as

$$\hat{G} = \frac{3.5458\text{e-}006s^2 - 0.0046s - 3.5304813}{0.3573s^2 - 28.9306s - 2.32566e004} \qquad (17)$$

The poles of the second order model reduced system lie at $+300.5, -219.6$ rad/s while the poles of the model using the designed stiffness were at ± 266.9 rad/s. Fig.6 shows the Bode magnitude plot of the higher order ID model and the final reduced order model.

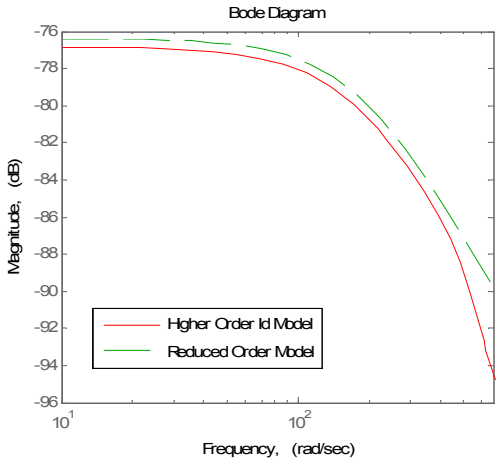

Fig.6. Bode magnitude plot of the higher order Id model and the final reduced order model.

Comparing (15) and (17), it can be observed that there are some additional frequency dependent terms in the reduced order transfer function. These terms likely appear due to eddy-current damping due to motion of magnets near conductors, magnetic coupling between actuator and sensor and unmodeled dynamics in the amplifiers and data acquisition system. The numerator and denominator are multiplied by a common factor so that the leading coefficient in the denominator polynomial matches the levitating mass, m. Then the constant term, equal to $23{,}257\ [\text{Nm}^{-1}]$, corresponds to the estimated axial stiffness. This shows a variation of about 8.6 % from the designed stiffness value of $25{,}450\ [\text{Nm}^{-1}]$ which is normal in magnetic bearing design.

VI. Conclusion

In this paper, we design a novel experimental apparatus with one degree of freedom and complete magnetic levitation to study the artificial heart for power minimization and control. We also present the various design intricacies so that apparatus can be easily reproduced in other laboratories. Modeling of the system is carried out together with validation by system identification tools for designing controllers. We also show application of the virtual zero power controller to stabilize the system. In the end, we present a discussion on system identification methods that can be used for problems of similar nature. Future work would focus on developing sophisticated controllers to handle quasi-periodic disturbances as seen in the natural heart and minimize power of the actuator. Approaches to be explored are nonlinear internal model control and iterative learning control. These controllers will find extensive applications in artificial hearts in the near future and lead to significant benefits in terms of cost and comfort to the patients.

References

[1] J.Antaki, B. Paden, S. Banda, M. Piovoso, "Award winning control applications," *IEEE Control Systems Magazine*, Vol. 22, No. 6, pp. 8- 20, Dec. 2002.

[2] B. Paden, N. Groom, J. Antaki , "Design Formulas for Permanent-Magnet Bearings", *Journal of Mechanical Design*, vol. 125, December, pp 734 – 738, Dec. 2003.

[3] J. P. Yonnet, G. Lemarquand, S. Hemmerlin, & E. Olivierr-Rullliere, "Stacked Structures of Passive Magnetic Bearings", *Journal of Applied Physics*, 70 (10), pp 6633 – 6635, Nov. 1991.

[4] S. Earnshaw, "On the nature of the molecular forces which regulate the constitution of the luminferous ether", Trans. Camb. Phil. Soc., 7, pp 97-112, 1842.

[5] J. Lyman, "Virtually zero powered suspension", U.S. Patent 3 860 300, 1975.

[6] B. Paden, J. F. Antaki and N. Groom, 1999,"Animal trials of a magnetically levitated left-ventricular assist device," 5th International Symposium on Magnetic Suspension Technology, Santa Barbara CA, pp. 251-258, Dec. 1999.

[7] G. Gloth, M. Sinapius, "Analysis of swept-sine runs during modal identification", *Mechanical systems and signal processing*, vol. 18, pp 1421 – 1441, Nov. 2004.

[8] L. Ljung, *System identification: Theory for the user*. Englewood Cliffs, NJ: Prentice-Hall, 1987.

[9] R. Johansson., *System modeling and Identification.* Englewood Cliffs, NJ: Prentice-Hall, 1993.

[10] U. Forsell, L. Ljung, "Closed-loop identification revisited", *Automatica*, vol. 35, pp 1215 – 1241, Jan. 1999.

[11] Quanser Consulting Inc., *Q8 Data acquisition system user's guide*, version 1.0, 2003.

[12] Kaman measuring systems, *KD 2440 User's manual*, 1998..T.

[13] C. Kenney, G. Hewer, "Necessary and sufficient condition for balancing unstable systems", *IEEE transactions on Automatic Control*, 32(2), pp 157 – 160, 1987.

[14] J. Yang, C. S. Chen, J. A. De Abreu-Garcia, Y. Xu, "Model reduction for unstable systems", *International Journal of Systems Science*, Vol. 24, No. 12, pp 207 – 214, 1993.

[15] A. Zilouchian, "Balanced structures and model reduction of unstable systems", in *Proc. IEEE Southeast Conf.*, Vol. 2, pp. 1198 - 1201, 1991

[16] C. Knospe, "The Nonlinear Control Benchmark Experiment", *Proceedings of the American Control Conference*, Chicago, pp 2134 - 2138, June 2000.